Seismicity and geometry of the south Chilean subduction zone (41.5°S–43.5°S): Implications for controlling parameters

D. Lange,[1] A. Rietbrock,[2] C. Haberland,[1] K. Bataille,[3] T. Dahm,[4] F. Tilmann,[5] and E. R. Flüh[6]

Received 22 December 2006; revised 13 February 2007; accepted 19 February 2007; published 29 March 2007.

[1] In 2005 an amphibious seismic network was deployed on the Chilean forearc between 41.75°S and 43.25°S. 364 local events were observed in a 11-month period. A subset of the P and S arrival times were inverted for hypocentral coordinates, 1-D velocity structure and station delays. Main seismic activity occurred predominantly in a belt parallel to the coast of Chiloé Island in a depth range of 12–30 km presumably related to the plate interface. The 30° inclination of the shallow part of the Wadati-Benioff zone is similar to observations further north indicating that oceanic plate age is not controlling the subduction angle of the shallower part for the Chilean subduction zone. The down-dip termination of abundant intermediate depth seismicity at approximately 70 km depth seems to be related to the young age (and high temperature) of the oceanic plate. Crustal seismicity is associated with the Liquiñe-Ofqui fault zone and active volcanoes. **Citation:** Lange, D., A. Rietbrock, C. Haberland, K. Bataille, T. Dahm, F. Tilmann, and E. R. Flüh (2007), Seismicity and geometry of the south Chilean subduction zone (41.5°S–43.5°S): Implications for controlling parameters, *Geophys. Res. Lett.*, *34*, L06311, doi:10.1029/2006GL029190.

1. Introduction

[2] The western South American margin is an outstanding example of a large-scale ocean-continent collision zone. The oceanic Nazca plate subducts beneath the South American continent beginning at the Chile Triple junction at 46°S and ending at the Cocos-Nazca spreading center at ~4°N. Several structural and physical parameter change over the ~5400 km long, North-South trending margin and lead to different geometry, behavior and coupling characteristics of the subduction zone. While in the last decade the northern and central part of this subduction zone has been intensively studied the southern part has attracted less attention, which might be caused by its difficult accessibility and lower seismic activity. However, the southern part exhibits strong seismic and tsunamogenic potential [*Cisternas et al.*, 2005] with the prominent example of the May 22, 1960 Valdivia earthquake (Mw = 9.5). The rupture length was approximately 1000 km starting at 37°S and stopping at 46.5°S, where the active Chile Rise is currently subducting beneath the South American plate [e.g., *Cifuentes*, 1989; *Cisternas et al.*, 2005].

[3] Recently, the nucleation area of the 1960 Valdivia earthquake (~37°S) has been studied using microseismicity and seismic refraction and reflection profiles, revealing the detailed structure of the Chilean forearc and the seismogenic zone [*Bohm et al.*, 2002; *Haberland et al.*, 2006]. However, little or none is known of the microseismicity and deeper structure of the forearc further to the South. Here we present new data from an amphibious seismic array located between 41.5–43.5°S reaching from the trench to the active magmatic arc incorporating the Island of Chiloé (Figure 1). It allows us to constrain the geometry of the subducting Nazca plate and seismogenic processes in the middle of the rupture area of the Valdivia earthquake. In the study area the age of the subducting Nazca plate is 18 ma [*Müller et al.*, 1997] and presently subducting obliquely beneath South America. The subducting Nazca plate in our study area is young, hot and buoyant close to the Chile Triple junction and was thus assumed to possibly subduct at low angles. Additionally, the overriding plate in the continental part of the study area is crossed by the 1000 km long NS trending Liquiñe-Ofqui fault zone (LOFZ) which is an transpressional dextral intra-arc shear zone [*Cembrano et al.*, 2002].

2. Experiment and Data

[4] In December 2004 we installed a seismic array of 18 three-component, short-period stations in southern Chile between 41.75°S and 43.25°S reaching from the coastline to the active volcanic arc. The stations were located on Chiloé Island, the continental forearc, and on some of the islands in the Golf of Ancud (Figure 1). In February 2005 additional 10 three-component, short-period ocean bottom seismometers (OBS) and 10 ocean bottom hydrophones (OBH) were installed West of Chiloé Island extending the seismic array to the West beyond the trench. The complete network was dismantled in October 2005 yielding to a total observation period of nearly 11 months. All land stations and OBS/OBH recorded continuously with a sampling rate of 0.01 s and 0.02 s, respectively.

3. Data Processing and 1D Velocity Model

[5] Automatic event detection using a LTA/STA algorithm was carried out on the continuous data stream. Event association was done independently on the offshore and

[1]Institute of Geosciences, University of Potsdam, Potsdam, Germany.
[2]Department of Earth and Ocean Sciences, University of Liverpool, UK.
[3]Departamento de Ciencias de la Tierra, Universidad de Concepción, Concepción, Chile.
[4]Institute of Geosciences, University of Hamburg, Hamburg, Germany.
[5]Bullard Laboratories, Department of Earth Sciences, University of Cambridge, Cambridge, UK.
[6]Leibniz-Institut für Meereswissenschaften an der Universität Kiel, Kiel, Germany.

0094-8276/07/2006GL029190

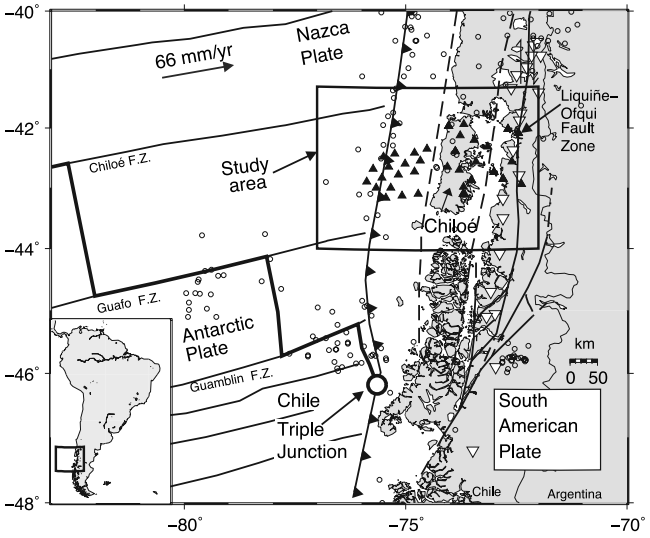

Figure 1. Tectonic map of the southeast Pacific and southern Chile close to the Chile triple junction modified after *Thomson* [2002]. Seismic stations and earthquake locations from the NEIC PDE Catalogue (1990–2006) are indicated by black triangles and open circles, respectively. The direction and velocity of the Nazca plate after *Angermann et al.* [1999]. Dashed line indicates the extent of subsidence associated with the 1960 Chile earthquake after *Plafker and Savage* [1970]. Volcanoes are indicated with inverted white triangles.

onshore networks using a network coincidence criterion. Furthermore, all waveforms were inspected visually by an analyst to search for weak events. In total 364 local events could be analyzed. Determination of accurate arrival times and initial locations was done manually using the software package GIANT [*Rietbrock et al.*, 1998], leading to a total of 7.698 arrival times (P: 4.141, S: 3.557). We determined simultaneously a local one dimensional (1D) velocity model, station corrections and accurate locations performing a joint inversion of the picked travel times [*Kissling et al.*, 1994]. We only included events with more than 8 onset times, containing at least 4 S wave observations, and a GAP (= largest azimuth range with no observations) $\leq$180°. This reduced the number to 98 well constrained events consisting out of 1.287 P- and 1.044 S-wave travel time observations. For computational reasons the elevation (depth) of the OBS/OBH stations was set to sea level, and the resulting travel time error compensation is accomplished by the simultaneous inversion of station correction terms [*Husen et al.*, 1999]. We first inverted a minimum RMS 1-D P wave velocity model using a constant v_p/v_s ratio of 1.77 derived from Wadati diagrams. A wide range of initial P wave velocity models (indicated in Figure 2) was used to investigate the quality and stability of the final minimum P wave velocity model. Then we determined the minimum 1-D S-wave velocity model by an additional series of inversions with different initial v_p/v_s ratios following *Husen et al.* [1999].

[6] In the upper crust P-wave velocities between 5.1 km/s and 5.8 km/s are estimated, which steadily increase to 7.8 km/s at 30 km depth. Velocities of 7.8 km/s and greater are found already at 30 km depth, which are at a shallower level than to the North at 38°S, where this transition is found at a depth of 55 km [*Bohm et al.*, 2002; *Haberland et al.*, 2006]. The velocity layers below 60 km are poorly resolved because of the reduced seismicity in greater depths. Due to near vertical ray paths at shallow depths the uppermost layers down to 15 km depth are not properly constrained. Inverted station delay times are smaller then 0.5 s, taking into account the static corrections introduced by the station elevation. All earthquakes having more than 8 observed onset times were relocated in our new minimum 1D velocity model resulting in 245 well located events (Figure 3).

[7] In order to estimate the accuracy of the obtained hypocenters (GAP $\leq$ 180°) we performed jackknife tests, i.e. we randomly selected subsets of observations (picks) for

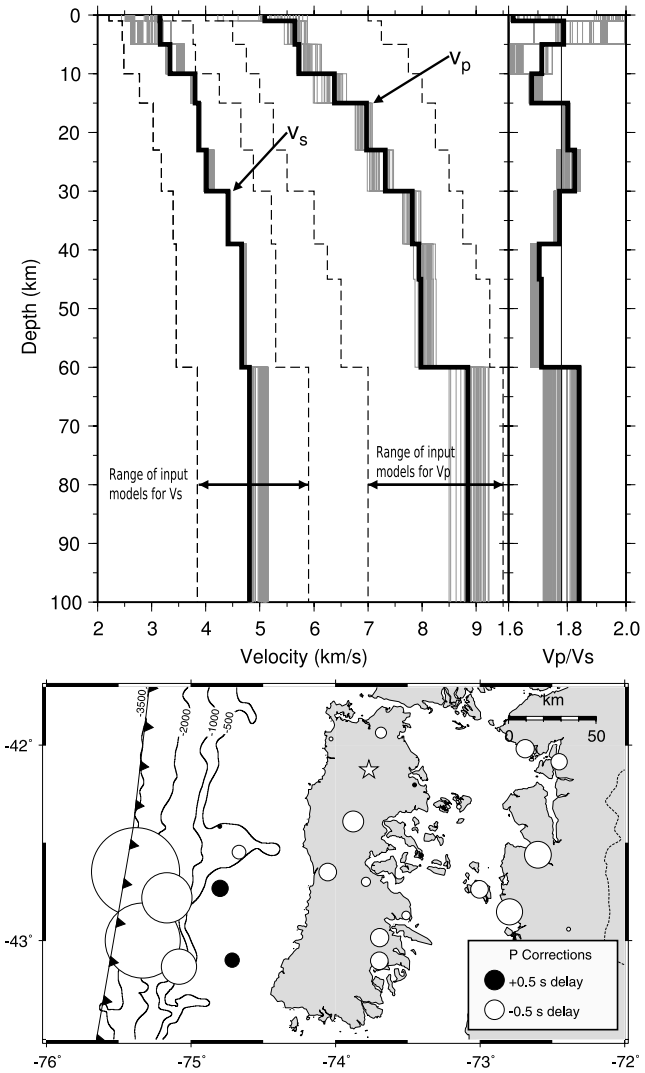

Figure 2. (top) Resulting velocity model and (bottom) station delays. The top plot shows models that fit the data equally well (best 3%) are plotted in gray. Range of input models for P and S velocity covering the velocity space between the two dashed lines. On the right, final v_p/v_s ratios are shown. The bottom plot shows corresponding station corrections for P-wave onset. The reference station is marked with a star and only stations corrections with more than 15 P onsets are shown. Bathymetry after *Smith and Sandwell* [1997].

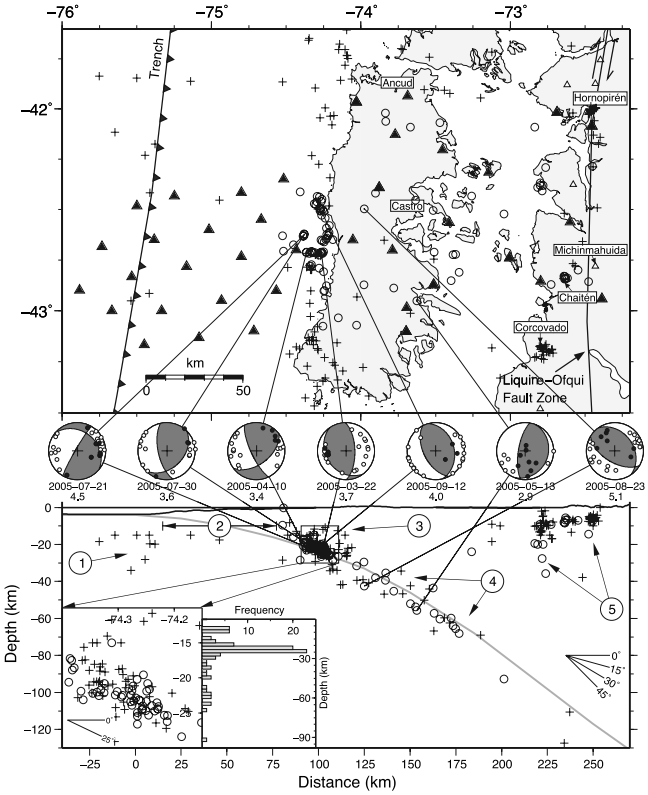

Figure 3. (top) Distribution of 245 located earthquakes. Hypocenters with GAP $\leq 180°$ (GAP $> 180°$) are depicted by circles (crosses). Black triangles mark seismic stations, volcanoes marked by upright white triangles. Middle: Fault plane solutions (lower hemisphere plot) based on first motion polarities and labeled with date and magnitude. (bottom) Hypocenters projected onto a E-W vertical cross-section clearly show the inclinated Wadati-Benioff zone (WBZ) and shallow crustal seismicity. Light gray line indicates interpreted possible top of subducting slab. Inlay plots show a close-up view of the seismicity beneath the coast and the depth-frequency distribution of events inside (GAP $\leq 180°$) the network. Numeration refers to the consecutive numbered text in Section 4.

certain (stronger) events and relocated them using the final velocity model. Using reduced subsets of 14 observations per event (which is the average number of observations per event of the data set used in the simultaneous inversion) we find an average standard deviation of 1.5 km which we assume to be representative for the hypocenter accuracy. Focal mechanisms for the strongest events were determined from first motion polarities [*Reasenberg and Oppenheimer*, 1985].

4. Seismicity and Geometry of the Slab

[8] The observed seismicity is clearly localized in different regions of the subduction zone between 12 and 70 km depth, and will be described from West to East following the subducting Nazca plate (see also numbers in Figure 3).

[9] 1. Seismicity at the trench is located between 12–34 km depth, which is well below the oceanic crust and presumably associated with mantle processes. Although a dense OBS/OBH network was in place no events larger than *Ml* = 3.3 and no seismicity associated with the oceanic crust were found.

[10] 2. Directly east of the trench a 70 km wide zone is observed in which only one event (*Ml* = 2.5) has been recorded. Similar sparse seismicity is also documented in the NEIC PDE catalogue (Figure 1) thus suggesting a long term aseismic behavior of this part of the seismogenic zone, associated with large slip (∼17 m) during the 1960 Valdivia earthquake [*Barrientos and Ward*, 1990].

[11] 3. Most events in our data set occurred below the western shore line of Chiloé Island in a depth range between 12 to 30 km depth. The observed seismicity in this region is mainly constituting of four larger events (*Ml* 4.0–4.4) and their associated aftershock sequences. These earthquakes are predominantly thrust type events as indicated by fault plane solutions. The epicenters mainly follow the curved course of the coast line. As clearly seen in the depth-frequency histogram (Figure 3), there is a pronounced drop in the seismicity rate below 30 km depth.

[12] 4. Below 30 km the subducting Nazca plate is depicted by seismicity down to a depth of 70 km. At 42 km depth a thrust event with *Ml* = 5.1 is located. However, all other events below 30 km are below *Ml* = 2, with an exception of an *Ml* = 2.9 thrust event at 55 km depth. Linear regression of events with GAP $\leq 180°$ and depths below 30 km (projected on a West-East cross-section) yield an inclination of 33(±3)° of the Wadati-Benioff zone (WBZ) (30° ± 1° for whole depth range).

[13] 5. High seismicity with events up to *Ml* 3.8 is found within the continental crust along the active volcanic arc (<20 km). The seismicity in this region is localized in several spatial clusters, two of them are linked to the volcanoes Corcovado and Chaitén (Figure 3). One cluster of 33 events is located 10 km south of Hornopirén with depths of less than 10 km along the LOFZ.

5. Discussion

[14] The presented micro seismicity from the amphibious local network reveals the first accurate image of the WBZ in the Southern Andes between 41.5° and 43.5°S. The downgoing Nazca plate is readily identifiable as an eastward dipping plane with an inclination of 30–33°. A similar dip (25–31°) of the WBZ seismicity has been found further to the north at 38°S [*Bohm et al.*, 2002; *Haberland et al.*, 2006], where 30 ma year old lithosphere is currently being subducted [*Müller et al.*, 1997]. In central Chile no significant lateral change of the subduction angle in the upper part of the subduction zone (≤45 km) can be noticed [*Suarez and Comte*, 1993; *Pardo et al.*, 2002]. *Pardo et al.* [2002] concluded that the shape at the initial part of the subduction seems to be independent of the age of the oceanic plate. Based on the presented seismicity and the observations of *Haberland et al.* [2006] we enlarge this conclusion to the southern Andes until 43°S. In this part the subducting Nazca plate is with 18 ma much younger than in the central Andes (between 22° and 30°S) with an age of 40 ma [*Müller et al.*, 1997]. Comparing the local seismicity by *Delouis et al.* [1996], *Bohm et al.* [2002], *Campos et al.* [2002], *Comte et al.* [2002], *Pardo et al.* [2002], *Haberland et al.* [2006] and this study give a further indication that at

least for the central and southern Chilean Subduction zone plate age and therefore temperature and density of the oceanic lithosphere are not controlling the initial subduction angle of the upper part ($\leq$45 km) of the downgoing plate.

[15] The highest seismicity rate is found 10 km to the west of Chiloé Island in a narrow band at a depth range of 12 km to 30 km (region 3 in Figure 3). The thrust-type character of these events and their shallow position allocate them in the coupling or seismogenic zone between the two plates, i.e. the zone rupturing in large earthquakes. However, since estimates for the width of the rupture plane of the 1960 earthquake range between 125 to 150 km [*Plafker and Savage*, 1970; *Barrientos and Ward*, 1990] we think that these events occur only in a certain part of the seismogenic zone. Accordingly, the aseismic region (region 2 in Figure 3) West of this zone of high seismicity might correspond to a region with aseismic frictional afterslip [*Hsu et al.*, 2006] or in a conditional stable regime [*Scholz*, 1998], which can accumulate substantial strain in the weak materials without complete creep relaxation [*Bilek and Lay*, 2002].

[16] Although the seismicity rate is dropping below 30 km depth (Figure 3, bottom) a clear down dip end of the seismogenic zone based on the seismicity distribution can hardly been defined. Taking only into account events with a GAP $\leq 180^\circ$ (circles in Figure 3) we would place the down dip end at about 25–30 km depth. The sparse events deeper than 30 to 50 km (region 4 in Figure 3) are most likely associated to intraplate (intermediate depth) seismicity as further North in Chile [*Campos et al.*, 2002; *Haberland et al.*, 2006]. However, it should be noted that two events (at 42 and 55 km depth) show thrust type mechanisms actually not anticipated for intraplate events at this depth range in the South American subduction zone where down dip extension along the slab is mostly observed. Since both events are clearly located inside the subducting slab, they could be indicative of dehydration processes in the subducting mantle, thought to be the cause for the occurrence of a double seismic zone in Northern Chile [*Comte et al.*, 1999; *Rietbrock and Waldhauser*, 2004]. Nevertheless, the seismicity diminishes significantly below 70 km depth. Further to the North intermediate depth (micro-) seismicity terminates at 120 km depth (at 38° S) [e.g., *Bohm et al.*, 2002] and reaches down to depths of 200 km in northern Chile [e.g., *Comte et al.*, 1999].

[17] It has been previously proposed that the intermediate depth earthquakes are related with phase transformations and dehydration reactions and are thus strongly temperature dependent [e.g., *Hacker et al.*, 2003]. The Cascadia subduction zone, where oceanic plate of similar age is being subducted, shows a similar depth distribution of the intermediate depth earthquakes [*Hacker et al.*, 2003]. We therefore associate the diminishing of the seismicity below 70 km depth to reflect the relatively high temperature of the downgoing slab at this latitude.

[18] Significant crustal seismicity (<20 km depth) along the arc-parallel LOFZ suggests the recent activity of this shear zone.

6. Conclusions

[19] Our data indicates that the age (and therefore temperature) of the oceanic plate is not a first-order controlling factor for the subduction angle of the shallower part of the subduction zone along the central and southern Chilean margin. However, in accordance with petrophysical models [*Hacker et al.*, 2003] the relatively high temperature of the oceanic plate at this latitude seems to control the occurrence (and the down-dip end) of the intermediate depth seismicity. Intense shallow seismicity can be associated to a lower or central part of the seismogenic zone (the interface between upper and lower plate rupturing in large earthquakes). Moderate seismicity in the continental crust is spatially related with young volcanoes and indicates recent activity of the LOFZ.

[20] **Acknowledgments.** The TIPTEQ seismic array was run collaboratively by the University of Potsdam, Germany, University of Liverpool, UK, University of Hamburg, Germany, the Universidad de Concepción, Chile and the IFM-GEOMAR, Germany. We gratefully acknowledge the cooperation of many Chilean landowners, companies, and institutions for support and for allowing us to install the seismic station on their property. Furthermore we thank all field crews for their excellent work under difficult conditions, especially G. Hermosilla, M. Piña, M. Moreno, J. Jarra, F. Sanchez, V. Venegas and M. Contreras. GIPP (GFZ) and IFM-GEOMAR provided instruments. We thank master and crew of R/V "SONNE" cruise SO 181 for the deployment of the OBS/OBH. This is publication GEOTECH-226 of the R&D-Programme GEOTECHNOLOGIEN funded by the German Ministry of Education and Research (BMBF) and German Research Foundation (DFG), grant 03G0594C.

References

Angermann, D., J. Klotz, and C. Reigber (1999), Space-geodetic estimation of the Nazca-South America Euler vector, *Earth Planet. Sci. Lett.*, *171*(3), 329–334.

Barrientos, S. E., and S. N. Ward (1990), The 1960 Chile earthquake: Inversion for slip distribution from surface deformation, *Geophys. J. Int.*, *103*, 589–598.

Bilek, S. L., and T. Lay (2002), Tsunami earthquakes possibly widespread manifestations of frictional conditional stability, *Geophys. Res. Lett.*, *29*(14), 1673, doi:10.1029/2002GL015215.

Bohm, M., S. Lüth, H. Echtler, G. Asch, K. Bataille, C. Bruhn, A. Rietbrock, and P. Wigger (2002), The Southern Andes between 36° and 40°S latitude: Seismicity and average seismic velocities, *Tectonophysics*, *356*, 275–289.

Campos, J., et al. (2002), A seismological study of the 1835 seismic gap in south-central Chile, *Phys. Earth Planet. Inter.*, *132*, 177–195.

Cembrano, J., A. Lavenu, P. Reynolds, G. Arancibia, G. López, and A. Sanhueza (2002), Late Cenozoic transpressional ductile deformation north of the Nazca–South America–Antarctica triple junction, *Tectonophysics*, *354*, 289–314.

Cifuentes, I. L. (1989), The 1960 Chilean earthquakes, *J. Geophys. Res.*, *94*(B1), 665–680.

Cisternas, M., et al. (2005), Predecessors of the giant 1960 Chile earthquake, *Nature*, *437*(15), 404–407, doi:10.1038/nature03943.

Comte, D., L. Dorbath, M. Pardo, T. Monfret, H. Haessler, L. Rivera, M. Frogneux, B. Glass, and C. Meneses (1999), A double-layered seismic zone in Arica, northern Chile, *Geophys. Res. Lett.*, *26*(13), 1965–1968.

Comte, D., H. Haessler, L. Dorbath, M. Pardo, T. Monfret, A. Lavenu, B. Pontoise, and Y. Hello (2002), Seismicity and stress distribution in the Copiapo, northern Chile subduction zone using combined on- and off-shore seismic observations, *Phys. Earth Planet. Inter.*, *132*, 197–217.

Delouis, B., A. Cisternas, L. Dorbath, L. Rivera, and E. Kausel (1996), The Andean subduction zone between 22 and 25°S (northern Chile): Precise geometry and state of stress, *Tectonophysics*, *259*, 81–100.

Haberland, C., A. Rietbrock, D. Lange, K. Bataille, and S. Hofmann (2006), Interaction between forearc and oceanic plate at the south-central Chilean margin as seen in local seismic data, *Geophys. Res. Lett.*, *33*, L23302, doi:10.1029/2006GL028189.

Hacker, B. R., S. M. Peacock, G. A. Abers, and S. D. Holloway (2003), Subduction factory: 2. Are intermediate-depth earthquakes in subducting slabs linked to metamorphic dehydration reactions?, *J. Geophys. Res.*, *108*(B1), 2030, doi:10.1029/2001JB001129.

Hsu, Y.-J., M. Simons, J.-P. Avouac, J. Galetzka, K. Sieh, M. Chlieh, D. Natawidjaja, L. Prawirodirdjo, and Y. Bock (2006), Frictional afterslip following the 2005 Nias-Simeulue earthquake, Sumatra, *Science*, *312*(5782), 1921–1926, doi:10.1126/science.1126960.

Husen, S., E. Kissling, E. Flueh, and G. Asch (1999), Accurate hypocentre determination in the seismogenic zone of the subducting Nazca Plate in

northern Chile using a combined on-/offshore network, *Geophys. J. Int.*, *138*(3), 687–701.

Kissling, E., W. L. Ellsworth, D. Eberhart-Phillips, and U. Kradolfer (1994), Initial reference models in local earthquake tomography, *J. Geophys. Res.*, *99*(B10), 19,635–19,646.

Müller, R. D., W. R. Roest, J.-Y. Royer, L. M. Gahagan, and J. G. Sclater (1997), Digital isochrons of the world's ocean floor, *J. Geophys. Res.*, *102*(B2), 3211–3214.

Pardo, M., D. Comte, and T. Monfret (2002), Seismotectonic and stress distribution in the central Chile subduction zone, *J. S. Am. Earth Sci.*, *15*(1), 11–22.

Plafker, G., and J. C. Savage (1970), Mechanism of the Chilean earthquakes of May 21 and 22, 1960, *Geol. Soc. Am. Bull.*, *81*, 1001–1030.

Reasenberg, P. A., and D. Oppenheimer (1985), Fpfit, fpplot, and fppage: FORTRAN computer programs for calculating and displaying earthquake fault-plane solutions, *U.S. Geol. Surv. Open File Rep. 85–739*.

Rietbrock, A., and F. Waldhauser (2004), A narrowly spaced double-seismic zone in the subducting Nazca plate, *Geophys. Res. Lett.*, *31*, L10608, doi:10.1029/2004GL019610.

Rietbrock, A., F. Scherbaum, and S. Malone (1998), The GIANT analysis system (graphical interactive aftershock network toolbox), *Seismol. Res. Lett.*, *69*(1), 40–45.

Scholz, C. H. (1998), Earthquakes and friction laws, *Nature*, *391*, 37–42.

Smith, W. H. F., and D. T. Sandwell (1997), Global sea floor topography from satellite altimetry and ship depth soundings, *Science*, *277*(5334), 1956–1962, doi:10.1126/science.277.5334.1956.

Suarez, G., and D. Comte (1993), Comment on "Seismic coupling along the Chilean Subduction Zone" by B. W. Tichelaar and L. R. Ruff, *J. Geophys. Res.*, *98*(B9), 15,825–15,828.

Thomson, S. N. (2002), Late Cenozoic geomorphic and tectonic evolution of the Patagonian Andes between latitudes 42°S and 46°S: An appraisal based on fission-track results from the transpressional intra-arc Liquiñe-Ofqui fault zone, *Geol. Soc. Am. Bull.*, *114*(9), 1159–1173.

K. Bataille, Departamento de Ciencias de la Tierra, Universidad de Concepción, Casilla 160-C, Concepción, Chile. (bataille@udec.cl)

T. Dahm, Institute of Geosciences, University of Hamburg, Bundesstr. 55, D-20146 Hamburg, Germany. (torsten.dahm@zmaw.de)

E. R. Flüh, IFM-GEOMAR, Wischhofstraße 1-3, D-24148 Kiel, Germany. (eflueh@ifm-geomar.de)

C. Haberland and D. Lange, Institute of Geosciences, University of Potsdam, Karl-Liebknecht-Straße 24, D-14476 Potsdam, Germany. (haber@geo.uni-potsdam.de; dietrich.lange@zmaw.de)

A. Rietbrock, Department of Earth and Ocean Sciences, University of Liverpool, 4 Brownlow Street, L69 3GP Liverpool, UK. (a.rietbrock@liverpool.ac.uk)

F. Tilmann, Bullard Laboratories, Department of Earth Sciences, University of Cambridge, Madingley Road, Cambridge CB3 0EZ, UK. (tilmann@esc.cam.ac.uk)